J. Cent. South Univ. (2021) 28: 3327−3339
DOI: https://doi.org/10.1007/s11771-021-4858-8

Springer

Thermal and concentration analysis of Phan-Thien-Tanner fluid flow due to ciliary movement in a peripheral layer

Khadija MAQBOOL[1], Sidra SHAHEEN[1], Elena BOBESCU[2], R. ELLAHI[1, 3]*

1. Department of Mathematics and Statistics, International Islamic University, Islamabad, Pakistan;
2. Department of Medical and Surgical Specialties, Faculty of Medicine, Transilvania University of Brasov, Brasov, Romania;
3. Fulbright Fellow Department of Mechanical Engineering, University of California Riverside, USA

Abstract: This paper presents the analysis of two-layer cilia induced flow of Phan-Thien-Tanner (PTT) fluid with thermal and concentration effect. The Phan-Thien-Tanner fluid model has been used in the analogy of mucus present in the respiratory tract. The two-layer model approach was used due to the Peri Ciliary liquid Layer (PCL) and Airway Ciliary Layer (ACL) present on the epithelium cell in respiratory tract. The mathematical modelling of two-layer flow problem was simplified using long wavelength and small Reynold's number approximation. The resulting differential equation with moving boundary gives exact solution for velocity, temperature and concentration profiles in two layers. The change in pressure has calculated by the results of velocity profile, also the pressure rise was evaluated by the numerical integration of pressure gradient along the channel wall. The impact of physical parameters on pressure rise, velocity, temperature and concentration profile was explained by the graphs. It can be seen from graphs that velocity and temperature profile are maximum in the inner layer of fluid (PCL) and concentration profile is maximum at outer layers of fluid (ACL).

Key words: ciliary flow; PTT fluid; two-layer model; thermal analysis; concentration effect

Cite this article as: Khadija MAQBOOL, Sidra SHAHEEN, Elena BOBESCU, R. ELLAHI. Thermal and concentration analysis of Phan-Thien-Tanner fluid flow due to ciliary movement in a peripheral layer [J]. Journal of Central South University, 2021, 28(11): 3327−3339. DOI: https://doi.org/10.1007/s11771-021-4858-8.

1 Introduction

From last fifty years, biologists and researchers precisely focused on the study of cilia and flagella motion. Cilia are hair like structures which are found in various physiological organs such as trachea, respiratory system, hair bundles on ears, fallopian tubes in women, lungs, kidneys, eyes and ependymal cell of brain that generates cerebrospinal flow. Cilia are divided into motile and non-motile cilia. Motile cilia have wave like motion which is responsible for the movement of fluid [1]. Motile cilia are also responsible for the propulsion of sperm in male reproductive system. Also, moving cilia keep the mucus airways clean from dirt, which are found in respiratory tract and irregularity in ciliary motion can result in serious respiratory, kidney and lung diseases [2 − 4]. In respiratory tract, ciliated epithelium is covered by airway surface liquid (ASL) and mainly consists of two different layers. The first one is mucus layer which is a non-homogenous, non-Newtonian, viscoelastic fluid and second layer is periciliary liquid layer (PCL) which

Received date: 2021-02-28; **Accepted date:** 2021-05-16
Corresponding author: R. ELLAHI, PhD, Professor; E-mail: rellahi@alumni.ucr.edu; ORCID: https://orcid.org/0000-0002-7805-8259

is considered as a less viscous fluid layer with small viscosity.

From the literatures [5 − 8], it is observed that cilia help to transport the complex biological fluid especially mucus clearance in the respiratory tract to transport the clear air into the lungs. The fresh air always move towards lungs by the periodic beating of cilia and with normal frequency of ciliary beat. A significant amount of research has been carried out in the field of ciliary motion and mucus transport, because mucus has been considered as Newtonian and non-Newtonian fluid. SIDDIQUI et al [9] discussed the motion of power law fluid in a tube with ciliated walls and showed the effect of power law index on pressure gradient and velocity profile, also he demonstrated in his study that velocity has increased for shear thinning fluid and decreased for shear thickening fluid. SIDDIQUI et al [10] postulated the Carreau fluid flow due to ciliary motion in a tube and axisymmetric flow of Carreau fluid model has been obtained by the perturbation method, also he showed that volume flow rate significantly changes by the Wessenberg number and cilia length parameter. NADEEM et al [11] analyzed the flow of Cu-blood nanofluid induced by metachronal wave motion of cilia inside a curved channel. NADEEM et al [12] considered the ciliary flow of Carreau fluid inside a symmetrical channel and obtained the analytical solution of problem by homotopy perturbation method (HPM) for the velocity, pressure and flow rate. AKBAR et al [13] investigated the effects of velocity and thermal slips on flow of Casson fluid caused by metachronal wave of cilia. MANZOOR et al [14] obtained exact solution for the motion of Jeffrey fluid inside a ciliated tube with porous medium and analyzed the viscoelastic effect on the ciliary flow. AKBAR et al [15] formulated a mathematical model for pressure driven flow of micro polar fluid induced by wavy motion due to ciliary beat and closed form solutions were obtained for axial and angular velocity, flow rate and pressure. Recently, SADAF et al [16] made an analysis for heat transfer of viscous fluid in a curved ciliated channel under the effect of magnetic field. BARTON et al [17] performed an investigation on muco-ciliar motion of fluid by assuming cilium as rod like structures. MILLER [18] examined the dynamical behavior of mucus transport in mechanically generated mucociliary system similar to that of mammals. This study laid down the foundation for the study of mucus transportation as well as particle movement in respiratory tract. ROSS et al [19] developed a mathematical model for two-layered muco ciliary motion of fluid. They assumed the mucus as viscoelastic fluid which forms the upper layer and other layer is assumed to be viscous fluid. AGARWAL et al [20] proposed a model for the study of planer mucus transport due to beating of cilia in the respiratory tract. They considered a two-layered model and observed an increase in transport of mucus with decrease in shear modulus of elasticity. NORTON et al [21] considered the mucus as Jeffrey and Maxwell fluid and formulated a mucus transport where the metachronal wave exhibits simplectic behavior. JAYATHILAKE et al [22] carried out a numerical study of mucus transport induced by the diseased cilia and found that there was a decrease in mucus velocity. SHAHEEN et al [23] considered mucus as Jeffrey nanofluid and investigated the flow caused by metachronal beating of cilia.

Thermal and concentration analysis is very important in biological flows, because biologically-inspired pumping systems (artificial cilia) have great applications in bioengineering due to high efficiency. Industrial applications of mass diffusion also contains feature of multi-phase (two-phase) flows. Few core studies of thermal and concentration analysis had been investigated in Refs. [24 − 26]. Besides these studies, SHAHEEN et al [27] analyzed the thermal and concentration gradient effects on the peristaltic motion of non-Newtonian Jeffrey fluid. ABDELSALAM et al [28] studied the theoretical analysis of thermal and concentration gradient on a fluid flowing due to ciliary motion with inclined magnetic field. Recently, several researchers [29 − 33] studied the effect of heat and mass transfer on biological fluids under the effects of different body forces. Two-layered flows have major applications in engineering and biomedical sciences. Therefore, CHEN et al [34] and AHMADPOUR et al [35] showed the numerical solutions of two-phase flows in different conduits. ABD et al [36] and MISRA et al [37] presented the mathematical analysis of

two-phase biological fluid flow for electromagnetic and power law fluid. The literature review [38−40] of muco ciliary flow tell us that thermal and concentration effect on viscous fluid flow due to ciliary movement in two-phase flow has not been addressed earlier, therefore, in this study, thermal and concentration effects on ciliary flow of PTT fluid was presented in peripheral layer. The novelty of the present work is to analyze the mucus flow trapping the viruses and dust particles in two layers ACL and PCL and influence of surrounding temperature and humidity.

Keeping in view, the importance of ciliary movement with reference to MCC (mucociliary clearance), we have considered the flow of mucus as Phan-Thien and Tanner fluid (PTT Model) in a symmetric ciliated channel under the effect of peripheral layer. The governing partial differential equations are modelled for velocity, temperature and concentration in two layers. The exact solutions for velocity, pressure, temperature and concentration are found in the present study for both layers PCL and ACL. The graphical results are included for the velocity, temperature and concentration distribution in both layers.

2 Mathematical model

We consider the two-dimensional channel flow of PTT fluids with distinct densities, viscosities, thermal conductivities and diffusion parameters in two immiscible fluid layers, i. e., ACL and PCL layers. The X-axis is taken along the direction of metachronal wave and Y-axis is perpendicular to it that is shown in Figure 1.

In symmetric channel, the cilia tips move in elliptical path therefore position of fluid particles is

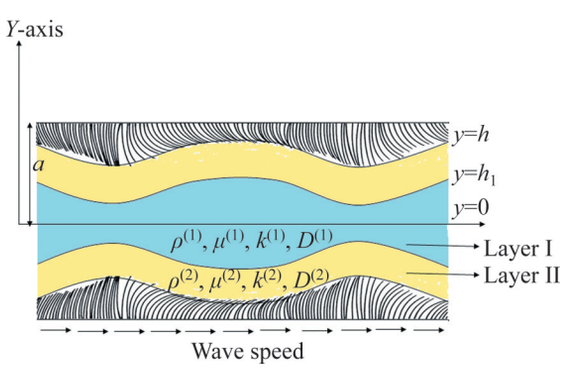

Figure 1 Geometry of problem

defined by the following expressions:

$$X^* = g\left(X^*, X_0^*, t^*\right)$$

$$= X_0^* + a\epsilon\alpha \sin\left(2\pi\left(\frac{X^* - ct^*}{\lambda}\right)\right) \tag{1}$$

$$Y^* = f\left(X^*, t^*\right) = a + a\epsilon\alpha \cos\left(2\pi\left(\frac{X^* - ct^*}{\lambda}\right)\right) \tag{2}$$

According to no slip condition of velocity, the velocities of cilia tips and fluid adjacent to cilia tips are same, therefore X^* and Y^* components of velocity are given as follows:

$$U^* = \left.\frac{\partial X^*}{\partial t^*}\right|_{X^* = X_0^*} = \frac{\partial g}{\partial t^*} + \frac{\partial g}{\partial X^*}\frac{\partial X^*}{\partial t^*} = \frac{\partial g}{\partial t^*} + \frac{\partial g}{\partial X^*}U^* \tag{3}$$

$$V^* = \left.\frac{\partial Y^*}{\partial t^*}\right|_{X^* = X_0^*} = \frac{\partial f}{\partial t^*} + \frac{\partial f}{\partial X^*}\frac{\partial X^*}{\partial t^*} = \frac{\partial f}{\partial t^*} + \frac{\partial f}{\partial X^*}U^* \tag{4}$$

Using Eqs. (1) − (2) into Eqs. (3) − (4), we arrive at

$$U^* = \frac{-\left(\frac{2\pi}{\lambda}\right)\left[\epsilon\alpha ac \cos\left(2\pi\left(\frac{X^* - ct^*}{\lambda}\right)\right)\right]}{1 - \left(\frac{2\pi}{\lambda}\right)\left[\epsilon\alpha a \cos\left(2\pi\left(\frac{X^* - ct^*}{\lambda}\right)\right)\right]} \tag{5}$$

and

$$V^* = \frac{-\left(\frac{2\pi}{\lambda}\right)\left[\epsilon\alpha ac \sin\left(2\pi\left(\frac{X^* - ct^*}{\lambda}\right)\right)\right]}{1 - \left(\frac{2\pi}{\lambda}\right)\left[\epsilon\alpha a \cos\left(2\pi\left(\frac{X^* - ct^*}{\lambda}\right)\right)\right]} \tag{6}$$

The wave frame and fixed frame are related by the following transformation:

$$x^* = X^* - ct^*,\ y^* = Y^*,\ u^* = U^* - c,\ v^* = V^*,$$
$$p^*(x, y) = P^*\left(X^*, Y^*, T\right) \tag{7}$$

where x^*, y^*, u^*, v^* and p^* are the quantities in wave frame and X^*, Y^*, U^*, V^* and P^* are in fixed frame.

For the transportation of two immiscible mucus layers in the airways, the continuity, momentum, heat and concentration equations can be written as:

$$\nabla \boldsymbol{V}^{(k)} = 0,\ k = 1, 2 \tag{8}$$

$$\rho^{(k)}\frac{\mathrm{d}\boldsymbol{V}^{(k)}}{\mathrm{d}t} = \mathrm{div}\boldsymbol{\tau}^{(k)},\ k = 1, 2 \tag{9}$$

$$\rho^{(k)}c_p^{(k)}\frac{\mathrm{d}T^{(k)}}{\mathrm{d}t}=\kappa^{(k)}\nabla^2T^{(k)}+\boldsymbol{\tau}^{(k)}\cdot\boldsymbol{L}^{(k)},\ k=1,\ 2 \tag{10}$$

$$\frac{\mathrm{d}C^{(k)}}{\mathrm{d}t}=D^{(k)}\nabla^2C^{(k)}+\frac{D_{kT}}{T_0}\nabla^2T^{(k)},\ k=1,\ 2 \tag{11}$$

$$\boldsymbol{V}^{(k)}=\left[u^{(k)}(x,\ y),\ v^{(k)}(x,\ y)\right] \tag{12}$$

Stress tensor for PTT fluid model is given by the following relation:

$$f\left(trace\left(\boldsymbol{\tau}^{(k)}\right)\right)\boldsymbol{\tau}^{(k)}+\lambda^{(k)}\hat{\boldsymbol{\tau}}^{(k)}=2\eta^{(k)}\boldsymbol{A}_1^{(k)} \tag{13}$$

where $\eta^{(k)}$, $\lambda^{(k)}$, $\boldsymbol{\tau}^{(k)}$, $\boldsymbol{A}_1^{(k)}$ represent the coeffiecient of viscosity, relaxation time, stress tensor and deformation rate of fluid in both layers.

$$\hat{\boldsymbol{\tau}}^{(k)}=\frac{\mathrm{d}\boldsymbol{\tau}^{(k)}}{\mathrm{d}t}-\boldsymbol{\tau}^{(k)}\cdot\boldsymbol{L}^{(k)}-\left(\boldsymbol{L}^{(k)}\right)^{\mathrm{T}}\cdot\boldsymbol{\tau}^{(k)} \tag{14}$$

$$f\left(trace\left(\boldsymbol{\tau}^{(k)}\right)\right)=1+\frac{\varepsilon^{(k)}\lambda^{(k)}}{\eta^{(k)}}trace\left(\boldsymbol{\tau}^{(k)}\right) \tag{15}$$

where superscript k denotes the fluids in two layers, $k=1$ shows the fluid in first layer and the fluid in second layer is represented by $k=2$. $\varepsilon^{(k)}$ denotes the elongation behavior parameter and $\lambda^{(k)}$ denotes the material parameters of fluids in both layers.

In the muco ciliary pumping, velocity, pressure and shear stress need to be analyzed, therefore continuity, momentum, heat and concentration equation together with the stress and strain relationship are expressed in the following manner:

$$\frac{\partial u^{(k)}}{\partial x}+\frac{\partial v^{(k)}}{\partial y}=0 \tag{16}$$

$$\rho^{(k)}\left(u^{(k)}\frac{\partial u^{(k)}}{\partial x}+v^{(k)}\frac{\partial u^{(k)}}{\partial y}\right)=-\frac{\partial p}{\partial x}+\frac{\partial\tau_{xx}^{(k)}}{\partial x}+\frac{\partial\tau_{xy}^{(k)}}{\partial y} \tag{17}$$

$$\rho^{(k)}\left(u^{(k)}\frac{\partial v^{(k)}}{\partial x}+v^{(k)}\frac{\partial v^{(k)}}{\partial y}\right)=-\frac{\partial p}{\partial y}+\frac{\partial\tau_{yx}^{(k)}}{\partial x}+\frac{\partial\tau_{yy}^{(k)}}{\partial y} \tag{18}$$

$$\rho^{(k)}c_p^{(k)}\left(u^{(k)}\frac{\partial T^{(k)}}{\partial x}+v^{(k)}\frac{\partial T^{(k)}}{\partial y}\right)=\kappa^{(k)}\left(\frac{\partial^2T^{(k)}}{\partial x^2}+\frac{\partial^2T^{(k)}}{\partial y^2}\right)+trace\left(\boldsymbol{\tau}^{(k)}\cdot\boldsymbol{L}^{(k)}\right) \tag{19}$$

$$\left(u^{(k)}\frac{\partial C^{(k)}}{\partial x}+v^{(k)}\frac{\partial C^{(k)}}{\partial y}\right)=D^{(k)}\left(\frac{\partial^2C^{(k)}}{\partial x^2}+\frac{\partial^2C^{(k)}}{\partial y^2}\right)+\frac{D_{KT}}{\left(T_1-T_0\right)}\left(\frac{\partial^2T^{(k)}}{\partial x^2}+\frac{\partial^2T^{(k)}}{\partial y^2}\right) \tag{20}$$

where stress tensors can be written as:

$$\left(1+\frac{\varepsilon^{(k)}\lambda^{(k)}}{\eta^{(k)}}trace\left(\boldsymbol{\tau}^{(k)}\right)\right)\tau_{xx}^{(k)}+\lambda^{(k)}\left(u^{(k)}\frac{\partial u^{(k)}}{\partial x}+v^{(k)}\frac{\partial v^{(k)}}{\partial y}\right)\tau_{xx}^{(k)}-2\lambda^{(k)}\left(\tau_{xx}^{(k)}\frac{\partial u^{(k)}}{\partial y}+\tau_{xy}^{(k)}\frac{\partial v^{(k)}}{\partial y}\right)=2\eta^{(k)}\frac{\partial u^{(k)}}{\partial x} \tag{21}$$

$$\left(1+\frac{\varepsilon^{(k)}\lambda^{(k)}}{\eta^{(k)}}trace\left(\boldsymbol{\tau}^{(k)}\right)\right)\tau_{xy}^{(k)}+\lambda^{(k)}\left(u^{(k)}\frac{\partial u^{(k)}}{\partial x}+v^{(k)}\frac{\partial v^{(k)}}{\partial y}\right)\tau_{xy}^{(k)}-2\lambda^{(k)}\left(\tau_{xx}^{(k)}\frac{\partial u^{(k)}}{\partial y}+\tau_{xy}^{(k)}\frac{\partial v^{(k)}}{\partial y}+\tau_{xy}^{(k)}\frac{\partial u^{(k)}}{\partial x}+\tau_{yy}^{(k)}\frac{\partial v^{(k)}}{\partial x}\right)=2\eta^{(k)}\left(\frac{\partial u^{(k)}}{\partial x}+\frac{\partial v^{(k)}}{\partial y}\right) \tag{22}$$

$$\left(1+\frac{\varepsilon^{(k)}\lambda^{(k)}}{\eta^{(k)}}trace\left(\boldsymbol{\tau}^{(k)}\right)\right)\tau_{yy}^{(k)}+\lambda^{(k)}\left(u^{(k)}\frac{\partial u^{(k)}}{\partial x}+v^{(k)}\frac{\partial v^{(k)}}{\partial y}\right)\tau_{yy}^{(k)}-2\lambda^{(k)}\left(\tau_{xy}^{(k)}\frac{\partial u^{(k)}}{\partial y}+\tau_{yy}^{(k)}\frac{\partial v^{(k)}}{\partial y}\right)=2\eta^{(k)}\frac{\partial u^{(k)}}{\partial y} \tag{23}$$

The biological flows are observed by velocity, temperature and concentration that are assumed to be maximum at the center line of the ciliated channel whereas at the interface of both layers shear stresses and velocities of fluids are equal as mentioned in Ref. [41], therefore boundary conditions for velocities and shear stress can be written in following manner:

$$\tau_{xy}^{(1)}=0\ \text{at}\ y=0 \tag{24a}$$

$$\tau_{xy}^{(1)}=\tau_{xy}^{(2)}\ \text{at}\ y=h_1 \tag{24b}$$

$$u^{(1)}=u^{(2)}\ \text{at}\ y=h_1 \tag{24c}$$

$$u^{(2)}=\frac{-\left(\frac{2\pi}{\lambda}\right)\left[\epsilon a\alpha c\sin\left(\frac{2\pi}{\lambda}\right)x\right]}{1-\left(\frac{2\pi}{\lambda}\right)\left[\epsilon a\alpha\cos\left(\frac{2\pi}{\lambda}\right)x\right]}\ \text{at}\ y=h \tag{24d}$$

$$v^{(2)} = \frac{\left(\frac{2\pi}{\lambda}\right)\left[\epsilon a\alpha c \sin\left(\frac{2\pi}{\lambda}\right)z\right]}{1-\left(\frac{2\pi}{\lambda}\right)\left[\epsilon a\alpha \cos\left(\frac{2\pi}{\lambda}\right)z\right]} \text{ at } y = h \tag{24e}$$

Similarly boundary conditions for temperature and concentration profile can be written as:

$$\frac{\partial T^{(1)}}{\partial y} = 0 \text{ at } y = 0 \tag{25a}$$

$$\kappa^{(1)}\frac{\partial T^{(1)}}{\partial y} = \kappa^{(2)}\frac{\partial T^{(2)}}{\partial y} \text{ at } y = h_1 \tag{25b}$$

$$T^{(1)} = T^{(2)} \text{ at } y = h_1 \tag{25c}$$

$$T^{(2)} = T_0 \text{ at } y = h \tag{25d}$$

$$\frac{\partial C^{(1)}}{\partial y} = 0 \text{ at } y = 0 \tag{26a}$$

$$D^{(1)}\frac{\partial C^{(1)}}{\partial y} = D^{(2)}\frac{\partial C^{(2)}}{\partial y} \text{ at } y = h_1 \tag{26b}$$

$$C^{(1)} = C^{(2)} \text{ at } y = h_1 \tag{26c}$$

$$C^{(2)} = C_0 \text{ at } y = h \tag{26d}$$

where

$$x^* = \frac{x}{\lambda},\ y^* = \frac{y}{a},\ u^{*(k)} = \frac{u^{(k)}}{c},\ v^{*(k)} = \frac{v^{(k)}}{\beta c},$$

$$h^* = \frac{h}{a},\ h_1{}^* = \frac{h_1}{a}, p^* = \frac{a\beta}{c\eta^{(1)}}p,\ \beta = \frac{a}{\lambda},$$

$$\tau_{ij}{}^{*(k)} = \frac{a}{\eta^{(1)}c}\tau^{(k)}{}_{ij},\ Re = \frac{\rho^{(1)}ac}{\eta^{(1)}},$$

$$Pr = \frac{\eta^{(1)}c_p}{\kappa^{(1)}},\ Br = \frac{\eta^{(1)}c^2}{\kappa^{(1)}\left(T_1 - T_0\right)},$$

$$\theta^{(k)} = \frac{T^{(k)} - T_0}{T_1 - T_0},\ \phi^{(k)} = \frac{C^{(k)} - C_0}{C_1 - C_0},\ S_H = \frac{\eta^{(1)}}{D^{(1)}\rho^{(1)}},$$

$$S_T = \frac{\rho^{(1)}D_{KT}}{\eta^{(1)}\left(C_1 - C_0\right)},\ \rho^{*(k)} = \frac{\rho^{*(k)}}{\rho^{(1)}},\ \delta = \frac{a_1}{a},$$

$$\eta^{*(k)} = \frac{\eta^{*(k)}}{\eta^{(1)}},\ \kappa^{*(k)} = \frac{\kappa^{*(k)}}{\kappa^{(1)}},\ D^{*(k)} = \frac{D^{*(k)}}{D^{(1)}} \tag{27}$$

After dropping "*", non-dimensional forms of Eqs. (16)–(26) are given as follows:

$$\frac{\partial u^{(k)}}{\partial x} + \frac{\partial v^{(k)}}{\partial y} = 0 \tag{28}$$

$$Re\left(u^{(k)}\frac{\partial u^{(k)}}{\partial x} + v^{(k)}\frac{\partial u^{(k)}}{\partial y}\right) = -\frac{\partial p}{\partial x} + \beta^2\frac{\partial \tau_{xx}^{(k)}}{\partial x} + \frac{\partial \tau_{xy}^{(k)}}{\partial y} \tag{29}$$

$$Re\beta^2\left(u^{(k)}\frac{\partial v^{(k)}}{\partial x} + v^{(k)}\frac{\partial v^{(k)}}{\partial y}\right) = -\frac{\partial p}{\partial y} + \beta^2\frac{\partial \tau_{yx}^{(k)}}{\partial x} + \beta\frac{\partial \tau_{yy}^{(k)}}{\partial y} \tag{30}$$

$$\beta\left(u^{(k)}\frac{\partial \theta^{(k)}}{\partial x} + v^{(k)}\frac{\partial \theta^{(k)}}{\partial y}\right) = \frac{\partial^2\theta^{(k)}}{\partial y^2} + \frac{Br}{\kappa^{(k)}}\tau_{yx}^{(k)}\frac{\partial u^{(k)}}{\partial y} \tag{31}$$

$$\beta\left(u^{(k)}\frac{\partial C^{(k)}}{\partial x} + v^{(k)}\frac{\partial C^{(k)}}{\partial y}\right) = \frac{\partial^2\phi^{(k)}}{\partial y^2} + \frac{S_H S_T}{D^{(k)}}\frac{\partial^2\theta^{(k)}}{\partial y^2} \tag{32}$$

$$\left(1 + \frac{\varepsilon^{(k)}\lambda^{(k)}}{\eta^{(k)}}trace\left(\boldsymbol{\tau}^{(k)}\right)\right)\tau_{xx}^{(k)} + \lambda^{(k)}\left(\beta u^{(k)}\frac{\partial u^{(k)}}{\partial x} + \beta^2 v^{(k)}\frac{\partial v^{(k)}}{\partial y}\right)\tau_{xx}^{(k)} - 2\lambda^{(k)}\left(\beta\tau_{xx}^{(k)}\frac{\partial u^{(k)}}{\partial x} + \beta^2\tau_{xy}^{(k)}\frac{\partial v^{(k)}}{\partial x}\right) = 2\beta\eta^{(k)}\frac{\partial u^{(k)}}{\partial x} \tag{33}$$

$$\left(1 + \frac{\varepsilon^{(k)}\lambda^{(k)}}{\eta^{(k)}}trace\left(\boldsymbol{\tau}^{(k)}\right)\right)\tau_{xy}^{(k)} + \lambda^{(k)}\left(\beta u^{(k)}\frac{\partial u^{(k)}}{\partial x} + \beta^2 v^{(k)}\frac{\partial v^{(k)}}{\partial y}\right)\tau_{xy}^{(k)} - 2\lambda^{(k)}\left(\tau_{xx}^{(k)}\frac{\partial u^{(k)}}{\partial y} + \beta^2\tau_{xy}^{(k)}\frac{\partial v^{(k)}}{\partial y} + \beta\tau_{xy}^{(k)}\frac{\partial u^{(k)}}{\partial x} + \beta^2\tau_{yy}^{(k)}\frac{\partial v^{(k)}}{\partial x}\right) = \eta^{(k)}\left(\frac{\partial u^{(k)}}{\partial y} + \beta^2\frac{\partial v^{(k)}}{\partial x}\right) \tag{34}$$

$$\left(1 + \frac{\varepsilon^{(k)}\lambda^{(k)}}{\eta^{(k)}}trace\left(\boldsymbol{\tau}^{(k)}\right)\right)\tau_{yy}^{(k)} + \lambda^{(k)}\left(\beta u^{(k)}\frac{\partial u^{(k)}}{\partial x} + \beta^2 v^{(k)}\frac{\partial v^{(k)}}{\partial y}\right)\tau_{yy}^{(k)} - 2\lambda^{(k)}\left(\tau_{xy}^{(k)}\frac{\partial u^{(k)}}{\partial y} + \beta\tau_{yy}^{(k)}\frac{\partial v^{(k)}}{\partial y}\right) = 2\eta^{(k)}\frac{\partial u^{(k)}}{\partial y} \tag{35}$$

Also boundary conditions for velocity, stress, temperature and concentration are given as follows:

$$\tau_{xy}^{(1)} = 0 \text{ at } y = 0 \tag{36a}$$

$$\tau_{xy}^{(1)} = \tau_{xy}^{(2)} \text{ at } y = h_1 \tag{36b}$$

$$u^{(1)} = u^{(2)} \text{ at } y = h_1 \tag{36c}$$

$$u^{(2)} = -1 - 2\pi\epsilon\alpha\beta\cos(2\pi x) \text{ at } y = h \tag{36d}$$

$$v^{(2)} = \pm 2\pi\epsilon\left(\sin(2\pi x) + 2\pi\epsilon\alpha\beta\sin(2\pi x)\cos(2\pi x)\right) \quad \text{at } y = h \tag{36e}$$

Similarly boundary conditions for temperature and concentration profile can be written as:

$$\frac{\partial\theta^{(1)}}{\partial y} = 0 \text{ at } y = 0 \tag{37a}$$

$$\kappa^{(1)}\frac{\partial\theta^{(1)}}{\partial y} = \kappa^{(2)}\frac{\partial\theta^{(2)}}{\partial y} \text{ at } y = h_1 \tag{37b}$$

$$\theta^{(1)} = \theta^{(2)} \text{ at } y = h_1 \tag{37c}$$

$$\theta^{(2)} = 0 \text{ at } y = h \tag{37d}$$

$$\frac{\partial\phi^{(1)}}{\partial y} = 0 \text{ at } y = 0 \tag{38a}$$

$$D^{(1)}\frac{\partial\phi^{(1)}}{\partial y} = D^{(2)}\frac{\partial\phi^{(2)}}{\partial y} \text{ at } y = h_1 \tag{38b}$$

$$\phi^{(1)} = \phi^{(2)} \text{ at } y = h_1 \tag{38c}$$

$$\phi^{(2)} = 0 \text{ at } y = h \tag{38d}$$

where

$h(x) = \pm[1 + \epsilon\cos x]$, $h_1(x) = \pm[\delta + \delta\epsilon\cos x]$.

Using long wavelength and small Reynolds' number approximation ($Re \to 0$, $\beta \to 0$) [9, 10] in Eqs. (28−38), one can get the following expressions:

$$\frac{\partial p}{\partial x} = \frac{\partial\tau_{xy}^{(k)}}{\partial y} \tag{39}$$

$$\frac{\partial p}{\partial y} = 0 \tag{40}$$

$$\frac{\partial^2\theta^{(k)}}{\partial y^2} = -\frac{Br}{\kappa^{(k)}}\tau_{yx}^{(k)}\frac{\partial u^{(k)}}{\partial y} \tag{41}$$

$$\frac{\partial^2\phi^{(k)}}{\partial y^2} = -\frac{S_{\mathrm{H}}S_{\mathrm{T}}}{D^{(k)}}\frac{\partial^2\theta^{(k)}}{\partial y^2} \tag{42}$$

After using long wavelength approximation and solving Eqs. (33)−(35), one can write following expressions:

$$\tau_{xx}^{(k)} = 0 \tag{43}$$

$$\tau_{yy}^{(k)} = \frac{2\lambda^{(k)}}{\eta^{(k)}}\tau_{xy}^{2(k)} \tag{44}$$

$$\tau_{xy}^{(k)} + 2\frac{\varepsilon^{(k)}\lambda^{2(k)}}{\eta^{2(k)}}\tau_{xy}^{3(k)} = \eta^{(k)}\frac{\partial u^{(k)}}{\partial y} \tag{45}$$

with boundary conditions

$$\tau_{xy}^{(1)} = 0 \text{ at } y = 0 \tag{46a}$$

$$\tau_{xy}^{(1)} = \tau_{xy}^{(2)} \text{ at } y = h_1 \tag{46b}$$

$$u^{(1)} = u^{(2)} \text{ at } y = h_1 \tag{46c}$$

$$u^{(2)} = -1 - 2\pi\epsilon\alpha\beta\cos(2\pi x) \text{ at } y = h \tag{46d}$$

$$v^{(2)} = \pm 2\pi\epsilon\left(\sin(2\pi x) + 2\pi\epsilon\alpha\beta\sin(2\pi x)\cos(2\pi x)\right) \quad \text{at } y = h \tag{46e}$$

$$\frac{\partial\theta^{(1)}}{\partial y} = 0 \text{ at } y = 0 \tag{47a}$$

$$\kappa^{(1)}\frac{\partial\theta^{(1)}}{\partial y} = \kappa^{(2)}\frac{\partial\theta^{(2)}}{\partial y} \text{ at } y = h_1 \tag{47b}$$

$$\theta^{(1)} = \theta^{(2)} \text{ at } y = h_1 \tag{47c}$$

$$\theta^{(2)} = 0 \text{ at } y = h \tag{47d}$$

$$\frac{\partial\phi^{(1)}}{\partial y} = 0 \text{ at } y = 0 \tag{48a}$$

$$D^{(1)}\frac{\partial\phi^{(1)}}{\partial y} = D^{(2)}\frac{\partial\phi^{(2)}}{\partial y} \text{ at } y = h_1 \tag{48b}$$

$$\phi^{(1)} = \phi^{(2)} \text{ at } y = h_1 \tag{48c}$$

$$\phi^{(2)} = 0 \text{ at } y = h \tag{48d}$$

where $h(x) = \pm[1 + \epsilon\cos x]$, $h_1(x) = \pm[\delta + \delta\epsilon\cos x]$.

3 Solution of problem

To find the following stresses, one can make the integration of Eq. (39) w.r.t *"y"*

$$\tau_{xy}^{(k)} = \frac{\partial p}{\partial x}y + A_1^{(k)},\ k = 1, 2 \tag{49}$$

where $A_1^{(k)}$ are constants of integration.

Using conditions mentioned in Eq. (46a) into the above equation for k=1, it is found that $A_1^{(1)} = 0$.

$$\tau_{xy}^{(1)} = \frac{\partial p}{\partial x}y,\ 0 \leqslant y \leqslant h_1 \tag{50}$$

Similarly we use Eq. (46b) into Eq. (49) for $k = 2$ and find that $A_1^{(2)} = 0$.

$$\tau_{xy}^{(2)} = \frac{\partial p}{\partial x} y,\ h_1 \leqslant y \leqslant h \tag{51}$$

Expressions in Eqs. (50) and (51) clearly show that stresses $\tau_{xy}^{(k)}$ in both regions are same.

$$\tau_{xy}^{(k)} = \frac{\partial p}{\partial x} y \tag{52}$$

Substituting Eq. (52) into Eq. (43), one can write the following form:

$$\tau_{yy}^{(k)} = \frac{2\lambda^{(k)}}{\eta^{(k)}}\left(\frac{\partial p}{\partial x}\right)^2 y^2 \tag{53}$$

After using Eqs. (52) and (44), one can find the following form of velocity:

$$\frac{\partial u^{(k)}}{\partial y} = \frac{\partial p}{\partial x}\frac{y}{\eta^{(k)}} + 2\frac{\varepsilon^{(k)}\lambda^{2(k)}}{\eta^{3(k)}}\left(\frac{\partial p}{\partial x}\right)^3 y^3 \tag{54}$$

Integration of above equation yields the following form:

$$u^{(k)} = \frac{\partial p}{\partial x}\frac{y^2}{2\eta^{(k)}} + \frac{\varepsilon^{(k)}\lambda^{2(k)}}{\eta^{3(k)}}\left(\frac{\partial p}{\partial x}\right)^3 \frac{y^4}{2} + B^{(k)} \tag{55}$$

Using boundary conditions given in Eqs. (46a)–(46e) in above equation, one can get the following velocity profiles in two regions.

$$u^{(1)} = u(h) + \frac{\partial p}{\partial x}\frac{1}{2\eta^{(1)}}\left(y^2 - h_1^2\right) + \frac{\varepsilon^{(1)}\lambda^{2(1)}}{2\eta^{3(1)}}\left(\frac{\partial p}{\partial x}\right)^3 \cdot \left(y^4 - h_1^4\right) + + \frac{\partial p}{\partial x}\frac{1}{2\eta^{(2)}}\left(h_1^2 - h^2\right) + \frac{\varepsilon^{(1)}\lambda^{2(1)}}{2\eta^{3(1)}}\left(\frac{\partial p}{\partial x}\right)^3 \left(h_1^4 - h^4\right) \tag{56}$$

$$u^{(2)} = u(h) + \frac{\partial p}{\partial x}\frac{1}{2\eta^{(2)}}\left(y^2 - h^2\right) + \frac{\varepsilon^{(2)}\lambda^{2(2)}}{2\eta^{3(2)}}\left(\frac{\partial p}{\partial x}\right)^3 \cdot \left(y^4 - h^4\right) \tag{57}$$

After integrating Eq. (41) and using boundary conditions given in Eqs. (47a)–(47d), one can get following temperature profiles:

$$\theta^{(1)} = -\frac{Br}{12\kappa^{(1)}\eta^{(1)}}\left(\frac{\partial p}{\partial x}\right)^2 \left(y^4 - h_1^4\right) - \frac{2Br\varepsilon^{(1)}\lambda^{2(1)}}{30\kappa^{(1)}\eta^{3(1)}}\left(\frac{\partial p}{\partial x}\right)^4 \left(y^6 - h_1^6\right) - \frac{Br}{12\kappa^{(2)}\eta^{(2)}}\left(\frac{\partial p}{\partial x}\right)^2 \left(h_1^4 - h^4\right) - \frac{2Br\varepsilon^{(2)}\lambda^{2(2)}}{30\kappa^{(2)}\eta^{3(2)}}\left(\frac{\partial p}{\partial x}\right)^4 \left(h_1^6 - h^6\right) + \left(-\frac{Br}{3\eta^{(1)}}\left(\frac{\partial p}{\partial x}\right)^2 h_1^3 - \frac{2Br\varepsilon^{(1)}\lambda^{2(1)}}{5\eta^{3(1)}}\left(\frac{\partial p}{\partial x}\right)^4 h_1^5\right) \cdot \left(h_1 - h\right) + \left[-\frac{Br}{3\eta^{(2)}}\left(\frac{\partial p}{\partial x}\right)^2 h_1^3 - \frac{2Br\varepsilon^{(2)}\lambda^{2(2)}}{5\eta^{3(2)}}\left(\frac{\partial p}{\partial x}\right)^4 h_1^5\right]\left(h_1 - h\right) \tag{58}$$

$$\theta^{(2)} = -\frac{Br}{12\kappa^{(2)}\eta^{(2)}}\left(\frac{\partial p}{\partial x}\right)^2 \left(y^4 - h^4\right) - \frac{2Br\varepsilon^{(2)}\lambda^{2(2)}}{30\kappa^{(2)}\eta^{3(2)}}\left(\frac{\partial p}{\partial x}\right)^4 \left(y^6 - h^6\right) + \left(-\frac{Br}{3\eta^{(1)}}\left(\frac{\partial p}{\partial x}\right)^2 h_1^3 - \frac{2Br\varepsilon^{(1)}\lambda^{2(1)}}{5\eta^{3(1)}}\left(\frac{\partial p}{\partial x}\right)^4 h_1^5\right) \cdot \left(\frac{1}{\eta^{(2)}} - \frac{1}{\eta^{(1)}}\right)\left(y - h\right) \tag{59}$$

Similarly, Eq. (42) can be written as follows:

$$\phi^{(1)} = \frac{S_H{}^*S_T{}^*Br}{12D^{(1)}\kappa^{(1)}\eta^{(1)}}\left(\frac{\partial p}{\partial x}\right)^2 \left(y^4 - h_1^4\right) + \frac{2S_H{}^*S_T{}^*Br\varepsilon^{(1)}\lambda^{2(1)}}{30D^{(1)}\kappa^{(1)}\eta^{3(1)}}\left(\frac{\partial p}{\partial x}\right)^4 \left(y^6 - h_1^6\right) + \frac{S_H{}^*S_T{}^*Br}{12D^{(2)}\kappa^{(2)}\eta^{(2)}}\left(\frac{\partial p}{\partial x}\right)^2 \left(h_1^4 - h^4\right) + \frac{2S_H{}^*S_T{}^*Br\varepsilon^{(2)}\lambda^{2(2)}}{30D^{(2)}\kappa^{(2)}\eta^{3(2)}}\left(\frac{\partial p}{\partial x}\right)^4 \left(h_1^6 - h^6\right) + \left(\frac{S_H{}^*S_T{}^*Br}{3\kappa^{(1)}\eta^{(1)}}\left(\frac{\partial p}{\partial x}\right)^2 h_1^3 + \frac{2S_H{}^*S_T{}^*Br\varepsilon^{(1)}\lambda^{2(1)}}{30\kappa^{(1)}\eta^{3(1)}}\left(\frac{\partial p}{\partial x}\right)^4 h_1^5\right)\left(h_1 - h\right) - \left(\frac{S_H{}^*S_T{}^*Br}{3\kappa^{(2)}\eta^{(2)}}\left(\frac{\partial p}{\partial x}\right)^2 h_1^3 + \frac{2S_H{}^*S_T{}^*Br\varepsilon^{(2)}\lambda^{2(2)}}{30\kappa^{(2)}\eta^{3(2)}}\left(\frac{\partial p}{\partial x}\right)^4 h_1^5\right)\left(h_1 - h\right) \tag{60}$$

$$\phi^{(2)} = \frac{S_{\mathrm{H}}{}^*S_{\mathrm{T}}{}^*Br}{12D^{(2)}\kappa^{(2)}\eta^{(2)}}\left(\frac{\partial p}{\partial x}\right)^2 \left(y^4 - h^4\right) + \frac{2S_{\mathrm{H}}{}^*S_{\mathrm{T}}{}^*Br\varepsilon^{(2)}\lambda^{2(2)}}{30D^{(2)}\kappa^{(2)}\eta^{3(2)}}\left(\frac{\partial p}{\partial x}\right)^4 \left(y^6 - h^6\right) + \left[\frac{S_{\mathrm{H}}{}^*S_{\mathrm{T}}{}^*Br}{3\kappa^{(1)}\eta^{(1)}}\left(\frac{\partial p}{\partial x}\right)^2 h_1^3 +\right.$$

$$\frac{2S_{\mathrm{H}}{}^{*}S_{\mathrm{T}}{}^{*}Br\varepsilon^{(1)}\lambda^{2(1)}}{30\kappa^{(1)}\eta^{3(1)}}\left(\frac{\partial p}{\partial x}\right)^{4}h_1^{5}\Big](y-h)-$$

$$\Big[\frac{S_{\mathrm{H}}{}^{*}S_{\mathrm{T}}{}^{*}Br}{3\kappa^{(2)}\eta^{(2)}}\left(\frac{\partial p}{\partial x}\right)^{2}h_1^{3}+$$

$$\frac{2S_{\mathrm{H}}{}^{*}S_{\mathrm{T}}{}^{*}Br\varepsilon^{(2)}\lambda^{2(2)}}{30\kappa^{(2)}\eta^{3(2)}}\left(\frac{\partial p}{\partial x}\right)^{4}h_1^{5}\Big](y-h) \tag{61}$$

The total volumetric flow rate Q in dimensionless form is given by the following equation

$$Q=Q^{(1)}+Q^{(2)} \tag{62}$$

$$Q=2hu(h)+\left(\frac{h^3}{6\eta^{(1)}}-\frac{hh_1^2}{2\eta^{(1)}}-\frac{5h^3}{6\eta^{(2)}}+\frac{hh_1^2}{2\eta^{(2)}}\right)\frac{\partial p}{\partial x}+$$

$$\left(\frac{h^5\varepsilon^{(1)}\lambda^{2(1)}}{10\eta^{3(1)}}-\frac{hh_1^4\varepsilon^{(1)}\lambda^{2(1)}}{2\eta^{3(1)}}-\frac{9h^5\varepsilon^{(2)}\lambda^{2(2)}}{10\eta^{3(2)}}+\right.$$

$$\left.\frac{hh_1^4\varepsilon^{(2)}\lambda^{2(2)}}{2\eta^{3(2)}}\right)\left(\frac{\partial p}{\partial x}\right)^{3} \tag{63}$$

4 Graphical results

In this section the effects of involved parameters appearing in the immiscible PTT fluid flow induced by cilia motion are displayed through graphs. The effect of emerging parameters are observed on the pressure rise, velocity, temperature and concentration profile by fixing a=0.2, β=0.2, $\eta^{(1)}$=0.1, $\eta^{(2)}$=0.5, $\varepsilon^{(1)}$=0.1, $\varepsilon^{(2)}$=0.5, $\lambda^{(1)}$=0.1, $\lambda^{(2)}$=0.5, x=0.25, ϵ=0.25, p=2, δ=0.5, $\kappa^{(1)}$=0.1, $\kappa^{(2)}$=0.5, Br=1, $D^{(1)}$=0.1, $D^{(2)}$=0.5, S_{H}=1, S_{T}=1.

Figures 2(a)−(d) show the effects of various parameters on pressure rise for two immiscible fluids. These graphs show that with the increasing values of viscosities $(\eta^{(1)}, \eta^{(2)})$, pressure difference decreases in both layer and fluid becomes thick and more pressure is required to maintain the same flux. By increasing relaxation time $(\lambda^{(1)}, \lambda^{(2)})$, elastic forces become dominant over the viscous forces that result to grow the resistance in fluid layer and so pressure difference rises. Figures 3(a)−(d) show the effects of various parameters on velocity profiles for two immiscible fluids. These graphs show that velocity is maximum at the center of the tube and continuity is clearly shown in graphs at the interface of two fluids, i.e., $(x=0.5)$.

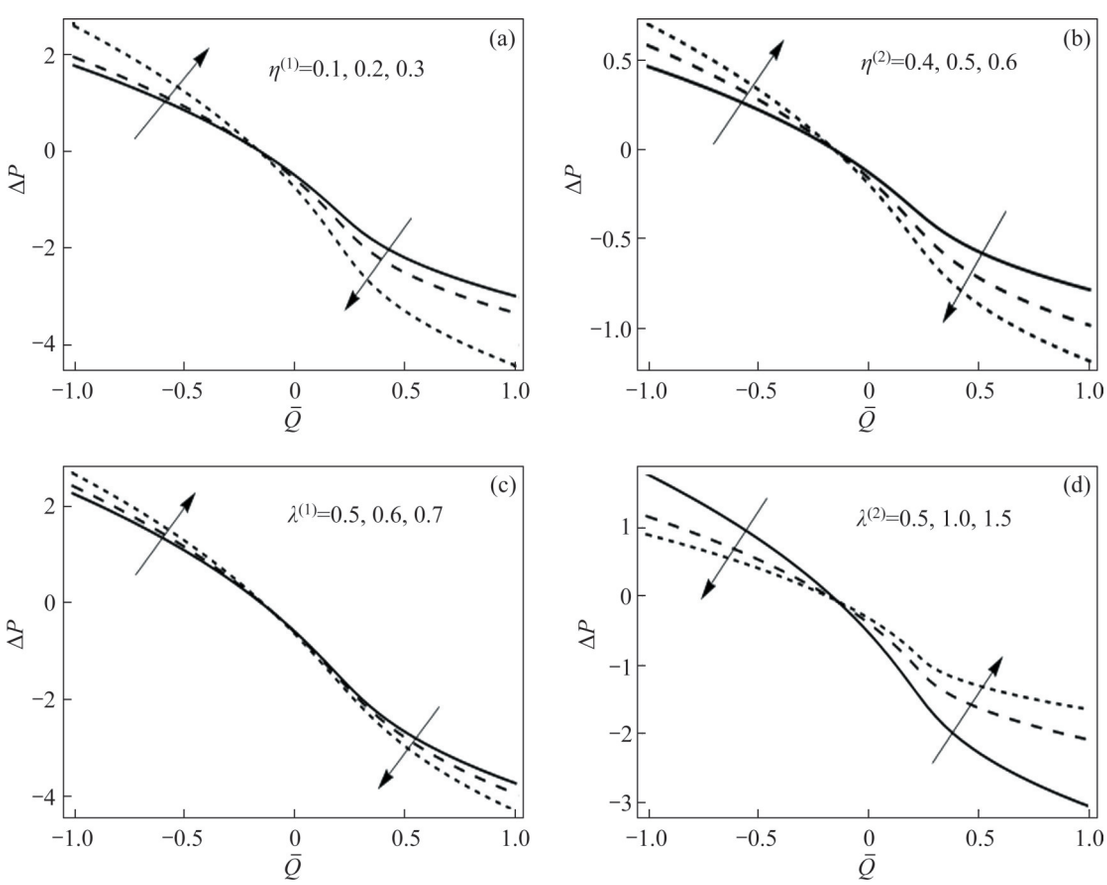

Figure 2 Effect of $\eta^{(1)}, \eta^{(2)}, \lambda^{(1)}$ and $\lambda^{(2)}$ on pressure rise

Figure 3(a) demonstrates the effect of distinct values of $\eta^{(1)}$ on the velocities of the fluids. It is observed that three curves in graph overlapped for the fluid in layer II. It is also clearly indicated by Eq. (57) that the expression $u^{(2)}$ does not involve the coefficient of viscosity $\eta^{(1)}$ for fluid in layer I, therefore the values of $\eta^{(1)}$ does not affect velocity of the fluid in layer II. However, the expressions (46) involve both parameters of viscosity, and velocities of both fluids are affected by varying the value of $\eta^{(2)}$ as shown in Figure 3(b). It is observed that with the increasing values of $\eta^{(2)}$ fluid become thick and the velocity profiles of the fluids appear slow.

Figures 3(d) and (d) show the effect of material parameters $\lambda^{(1)}$ and $\lambda^{(2)}$ on velocity profile in both regions. An increase in relaxation time produces considerable retardation in the mucus flow and elastic forces make the mucus thick by which the resistive property of mucus enhances which makes the flow slow. By increasing relaxation time $\lambda^{(1)}$, fluid decelerates in first region whereas it has no effect in second region, and by increasing $\lambda^{(2)}$, fluid velocity decreases in both the layers because the increase in relaxation time makes the fluid more viscous.

Figures 4(a) − (c) show the effects of various parameters on temperature profiles for two immiscible fluids. Figure 4(a) shows that by growing thermal conductivity $\kappa^{(1)}$, heat transfer decreases in first layer but it does not have any effect in second layer and $\kappa^{(2)}$ has the significant effect in both the layers because increase in thermal conductivity helps to reduce the rate of heat transfer in fluid, which can be seen in Figure 4(b). Figure 4(c) shows that with the increase in Brinkman number Br temperature profile decreases because the heat conduction from the boundary to the viscous fluid increases that reduces the rate of heat transfer.

Figures 5(a) − (d) show the effect of various parameters on concentration profiles for two immiscible fluids. Figure 5(a) shows that by increasing $D^{(1)}$, concentration profile decreases in first region because of the low diffusivity of the fluid in layer I but it does not have significant effect in second layer. Also $D^{(2)}$ has the noteworthy effect in both the layers because diffusivity of the fluid in layer II reduces the concentration profile in both

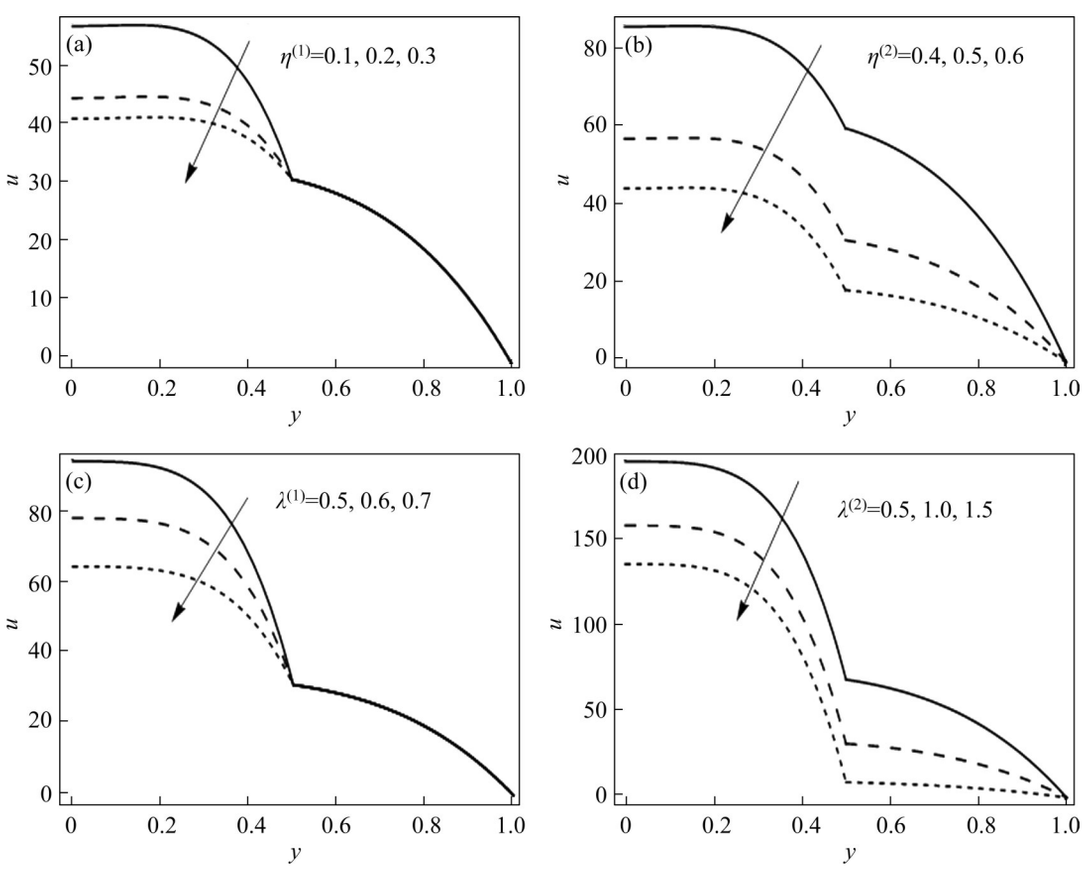

Figure 3 Effect of $\eta^{(1)}$, $\eta^{(2)}$, $\lambda^{(1)}$ and $\lambda^{(2)}$ on velocity profile

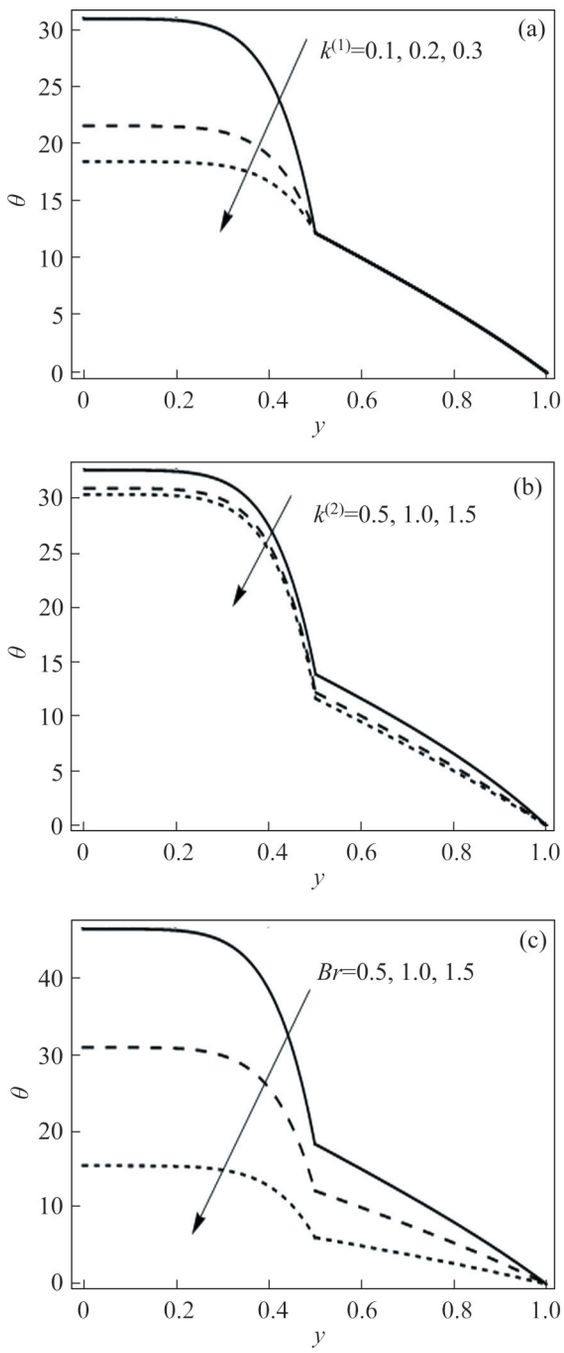

Figure 4 Effect of $k^{(1)}$, $k^{(2)}$ and Br on temperature profile

layers. Figures 5(c) and (d) show that by increasing S_H and S_T concentration profile decreases because momentum diffusivity is dominant over the mass diffusivity. It is also observed that mass flux due to temperature gradient resists the diffusion process.

5 Conclusions

The mathematical analysis of ciliary flow in two-layer model has been discussed in this research. The diffusive convective heat and mass transfer of ciliary flow in two-layer flow (liquid-liquid) is modelled with the help of mass, momentum, energy and concentration laws using linear PTT fluid model in both layers with different viscosities and densities. The momentum, energy and concentration equations are simplified under the lubrication approach.

Exact solutions for velocity, temperature and concentration profiles have been constructed for both layer and graphical results are also found by the help of software "MATHEMATICA". The flow features, e. g., pressure rise, velocity, temperature and concentration are analyzed for different values of involved parameters and following observations are noted.

1) Pressure rise surges in pumping region and falls in pumping region by increasing the values of viscosities of both fluid present in layer I and II and PTT fluid parameters of layer I but reverse behavior is observed for PTT fluid parameter in layer II.

2) Profiles of velocities, temperature and concentration show that fluid flow is continuous at the interface which is an essential requirement of continuum fluid.

3) It is noted that velocity of fluid decreases in first layer by increasing the viscosity and relaxation time of the fluid of phase I but flow decreases in both layer with the growing values of viscosity and relaxation time of fluid in phase II.

4) Temperature profile decays in layer I with the growing value of thermal conductivity of fluid in layer I but the heat transfer decays with the growing values of thermal conductivity and Brinkman number of fluid of phase II.

5) Concentration in the fluid of Phase I and II become slow with the growing values of $D^{(2)}$, S_H and S_T but concentration in fluid of Phase I decays $D^{(1)}$.

This study provides the results of mucus (PTT fluid) flow in a ciliated channel with two-phase flow in the presence of heat and concentration effects but effects of inertial forces and buoyancy forces are neglected in this study that will be considered in future research.

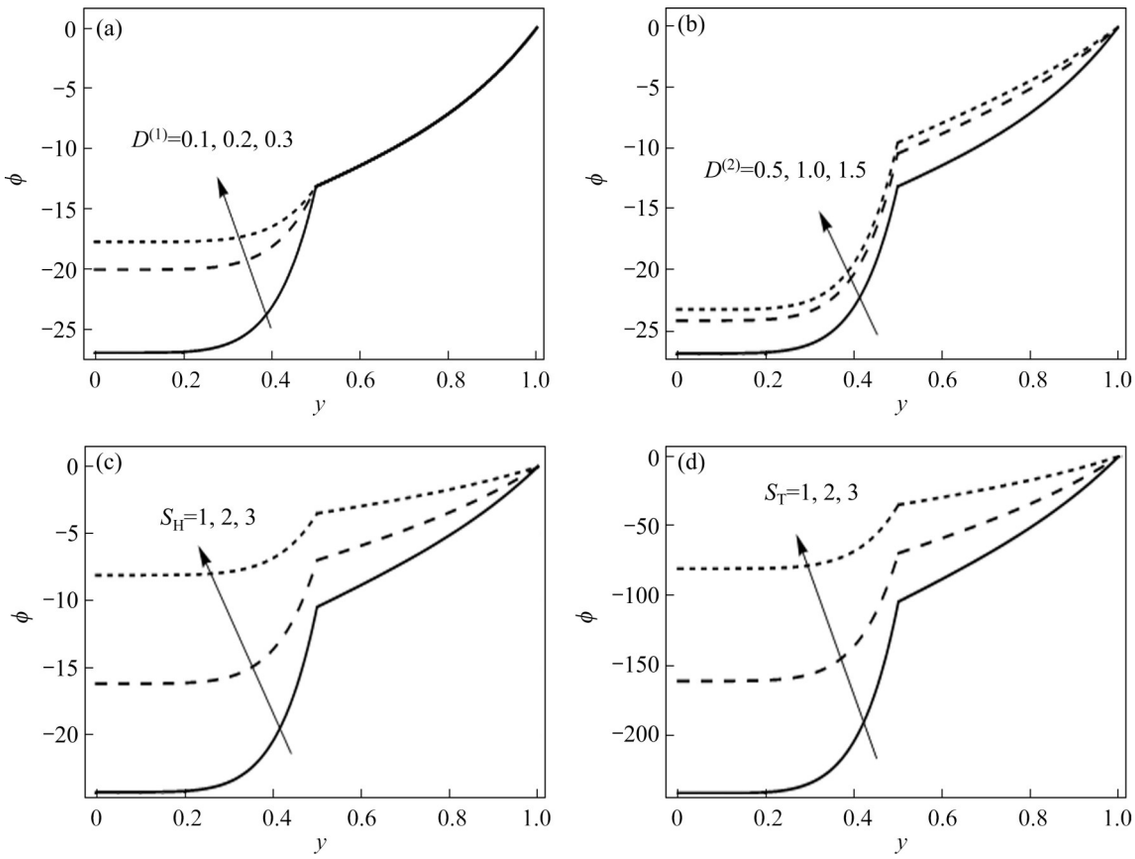

Figure 5 Effect of $D^{(1)}$, $D^{(2)}$, S_H and S_T on concentration profile

Nomenclature

$\boldsymbol{V}$	Velocity field vector
U, V	Velocity components in fixed frame
u, v	Velocity components in wave frame
X, Y	Rectangular coordinates of ciliated tube in fixed frame
x, y	Rectangular coordinates of ciliated tube in wave frame
$\eta^{(k)}$	Viscosity of fluid in two phases
P	Pressure in fixed frame
p	Pressure in wave frame
$\tau^{(k)}$	Cauchy stress tensor
$\boldsymbol{S}^{(k)}$	Shear rate
c	Wave speed
c_p	Specific heat capacity
$\varepsilon^{(k)}$	Elongation parameter
$\lambda^{(k)}$	Material parameter
ϵ	Cilia length
$\rho^{(k)}$	Density of fluid
α	Eccentricity of elliptical path
β	Wave numbe
$A_1{}^{(k)}$	Rivlin Erickson tensor
$T^{(k)}$	Temperature profile in two layers
T_0	Temperature at the center of the tube
T_1	Temperature at the ciliated wall
$C^{(k)}$	Concentration profile in two layers
C_0	Concentration profile at the center of the tube
C_1	Concentration at ciliated wall
D_B	Coefficient of mass diffusivity
D_T	Constant ratio due to thermal diffusion
Re	Reynolds' number
Br	Brinkman number
S_H	Schmidt number
S_T	Soret number

Contributors

Khadija MAQBOOL provided the model, reviewed and edited the final draft. Sidra

SHAHEEN used methodology to obtain the analytical results. Elena BOBESCU presented the validation of results. R. ELLAHI provided the formal analysis and handled the submission.

Conflict of interest

Khadija Maqbool, Sidra Shaheen, Elena Bobescu and R. Ellahi declare that they have no conflict of interest.

References

[1] SHANG Yi-dan, INTHAVONG K, TU Ji-yuan. Development of a computational fluid dynamics model for mucociliary clearance in the nasal cavity [J]. Journal of Biomechanics, 2019, 85: 74−83. DOI: 10.1016/j.jbiomech.2019.01.015.

[2] RUBIN B K. Secretion properties, clearance, and therapy in airway disease [J]. Translational Respiratory Medicine, 2014, 2: 6. DOI: 10.1186/2213-0802-2-6.

[3] KATHEM S H, MOHIELDIN A M, NAULI S M. The roles of primary cilia in polycystic kidney disease [J]. AIMS Molecular Science, 2014, 1(1): 27−46. DOI: 10.3934/molsci.2013.1.27.

[4] TILLEY A E, WALTERS M S, SHAYKHIEV R, CRYSTAL R G. Cilia dysfunction in lung disease [J]. Annual Review of Physiology, 2015, 77: 379 − 406. DOI: 10.1146/annurev-physiol-021014-071931.

[5] VÉLEZ-CORDERO J R, LAUGA E. Waving transport and propulsion in a generalized Newtonian fluid [J]. Journal of Non-Newtonian Fluid Mechanics, 2013, 199: 37 − 50. DOI: 10.1016/j.jnnfm.2013.05.006.

[6] HUSSONG J, LINDKEN R, FAULHAMMER P, NOREIKAT K, SHARP K V, KUMMER W, WESTERWEEL J. Cilia-driven particle and fluid transport over mucus-free mice tracheae [J]. Journal of Biomechanics, 2013, 46(3): 593−598. DOI: 10.1016/j.jbiomech.2012.08.020.

[7] GHEBER L, KORNGREEN A, PRIEL Z. Effect of viscosity on metachrony in mucus propelling cilia [J]. Cell Motility and The Cytoskeleton, 1998, 39(1): 9 − 20. DOI: 10.1002/(SICI)1097-0169(1998)39: 1<9: AID-CM2>3.0.CO;2-3.

[8] BUSTAMANTE-MARIN X M, OSTROWSKI L E. Cilia and mucociliary clearance [J]. Cold Spring Harbor Perspectives in Biology, 2017, 9(4): a028241. DOI: 10.1101/cshperspect.a028241.

[9] SIDDIQUI A M, HAROON T, RANI M, ANSARI A R. An analysis of the flow of a power law fluid due to ciliary motion in an infinite channel [J]. Journal of Biorheology, 2010, 24(2): 56−69. DOI: 10.1007/s12573-011-0026-3.

[10] SIDDIQUI A M, FAROOQ A A, RANA M A. An investigation of non-Newtonian fluid flow due to metachronal beating of cilia in a tube [J]. International Journal of Biomathematics, 2015, 8(2): 1550016. DOI: 10.1142/s1793524515500163.

[11] NADEEM S, SADAF H. Theoretical analysis of Cu-blood nanofluid for metachronal wave of cilia motion in a curved channel [J]. IEEE Transactions on NanoBioscience, 2015, 14(4): 447−454. DOI: 10.1109/TNB.2015.2401972.

[12] NADEEM S, MUNIM A, SHAHEEN A, HUSSAIN S. Physiological flow of Carreau fluid due to ciliary motion [J]. AIP Advances, 2016, 6(3): 035125. DOI: 10.1063/1.4945270.

[13] AKBAR N S, TRIPATHI D, BÉG O A, KHAN Z H. MHD dissipative flow and heat transfer of Casson fluids due to metachronal wave propulsion of beating cilia with thermal and velocity slip effects under an oblique magnetic field [J]. Acta Astronautica, 2016, 128: 1 − 12. DOI: 10.1016/j.actaastro.2016.06.044.

[14] MANZOOR N, MAQBOOL K, BÉG O A, SHAHEEN S. Adomian decomposition solution for propulsion of dissipative magnetic Jeffrey biofluid in a ciliated channel containing a porous medium with forced convection heat transfer [J]. Heat Transfer—Asian Research, 2019, 48(2): 556−581. DOI: 10.1002/htj.21394.

[15] AKBAR N S, TRIPATHI D, KHAN Z H, BÉG O A. Mathematical modelling of pressure-driven micropolar biological flow due to metachronal wave propulsion of beating cilia [J]. Mathematical Biosciences, 2018, 301: 121−128. DOI: 10.1016/j.mbs.2018.04.001.

[16] SADAF H, NADEEM S. Fluid flow analysis of cilia beating in a curved channel in the presence of magnetic field and heat transfer [J]. Canadian Journal of Physics, 2020, 98(2): 191−197. DOI: 10.1139/cjp-2018-0715.

[17] BARTON C, RAYNOR S. Analytical investigation of cilia induced mucous flow [J]. The Bulletin of Mathematical Biophysics, 1967, 29(3): 419 − 428. DOI: 10.1007/BF02476581.

[18] MILLER C E. An investigation of the movement of Newtonian liquids initiated and sustained by the oscillation of mechanical cilia [J]. Aspen Emphysema Conference, 1967, 10: 309−321.

[19] ROSS S M, CORRSIN S. Results of an analytical model of mucociliary pumping [J]. Journal of Applied Physiology, 1974, 37(3): 333−340. DOI: 10.1152/jappl.1974.37.3.333.

[20] AGARWAL M, SHUKLA J B. Mucus transport in the lung [J]. Mathematical and Computer Modelling, 1988, 11: 797−800. DOI: 10.1016/0895-7177(88)90603-6.

[21] NORTON M M, ROBINSON R J, WEINSTEIN S J. Model of ciliary clearance and the role of mucus rheology [J]. Physical Review E, 2011, 83: 011921. DOI: 10.1103/physreve.83.011921.

[22] JAYATHILAKE P G, LE D V, TAN Zhi-jun, LEE H P, KHOO B C. A numerical study of muco-ciliary transport under the condition of diseased cilia [J]. Computer Methods in Biomechanics and Biomedical Engineering, 2015, 18(9): 944−951. DOI: 10.1080/10255842.2013.864285.

[23] SHAHEEN S, MAQBOOL K, SIDDIQUI A M. Micro rheology of Jeffrey nanofluid through cilia beating subject to the surrounding temperature [J]. Rheologica Acta, 2020, 59(8): 565−573. DOI: 10.1007/s00397-020-01222-8.

[24] SAEED T, ABBAS I, MARIN M. A GL model on thermo-elastic interaction in a poroelastic material using finite element method [J]. Symmetry, 2020, 12(3): 488. DOI: 10.3390/sym12030488.

[25] ABRAR M N, SAGHEER M, HUSSIAN S. Entropy analysis of SWCNT & MWCNT flow induced by collecting beating of cilia with porous medium [J]. Journal of Central South University, 2019, 26(8): 2109 − 2118. DOI: 10.1007/s11771-019-4158-8.

[26] ZHANG Li-jun, ARAIN M B, BHATTI M M, ZEESHAN A, HAL-SULAMI H. Effects of magnetic Reynolds number on

swimming of gyrotactic microorganisms between rotating circular plates filled with nanofluids [J]. Applied Mathematics and Mechanics, 2020, 41(4): 637－654. DOI: 10.1007/s10483-020-2599-7.

[27] SHAHEEN A, HUSSAIN S, NADEEM S. Physiological flow of Jeffrey six constant fluid model due to ciliary motion [J]. Communications in Theoretical Physics, 2016, 66(6): 701−708. DOI: 10.1088/0253-6102/66/6/701.

[28] ABDELSALAM S I, BHATTI M M, ZEESHAN A, RIAZ A, BÉG O A. Metachronal propulsion of a magnetised particle-fluid suspension in a ciliated channel with heat and mass transfer [J]. Physica Scripta, 2019, 94(11): 115301. DOI: 10.1088/1402-4896/ab207a.

[29] ZAHER A Z, MOAWAD A M A, MEKHEIMER K S, BHATTI M M. Residual time of sinusoidal metachronal ciliary flow of non-Newtonian fluid through ciliated walls: Fertilization and implantation [J]. Biomechanics and Modeling in Mechanobiology, 2021, 20(2): 609－630. DOI: 10.1007/s10237-020-01405-5.

[30] ABO-ELKHAIR R E, BHATTI M M, MEKHEIMER K S. Magnetic force effects on peristaltic transport of hybrid bio-nanofluid (AuCu nanoparticles) with moderate Reynolds number: An expanding horizon [J]. International Communications in Heat and Mass Transfer, 2021, 123: 105228. DOI: 10.1016/j.icheatmasstransfer.2021.105228.

[31] ZHANG Li-jun, BHATTI M M, MARIN M, MEKHEIMER K S. Entropy analysis on the blood flow through anisotropically tapered arteries filled with magnetic zinc-oxide (ZnO) nanoparticles [J]. Entropy, 2020, 22(10): 1070. DOI: 10.3390/e22101070.

[32] ABBASI F M, ALSAEDI A, HAYAT T. Mixed convective heat and mass transfer analysis for peristaltic transport in an asymmetric channel with Soret and Dufour effects [J]. Journal of Central South University, 2014, 21(12): 4585－4591. DOI: 10.1007/s11771-014-2464-8.

[33] ABBASI F M, HAYAT T, AHMAD B, CHEN B. Peristaltic flow with convective mass condition and thermal radiation [J]. Journal of Central South University, 2015, 22(6): 2369−2375. DOI: 10.1007/s11771-015-2762-9.

[34] CHEN Wen-yi, WANG Jing-bo, JIANG Nan, ZHAO Bin, WANG Zhen-dong. Numerical simulation of gas-liquid two-phase jet flow in air-bubble generator [J]. Journal of Central South University of Technology, 2008, 15(1): 140−144. DOI: 10.1007/s11771-008-0333-z.

[35] AHMADPOUR M, SIAVASHI M, DORANEHGARD M H. Numerical simulation of two-phase flow in fractured porous media using streamline simulation and IMPES methods and comparing results with a commercial software [J]. Journal of Central South University, 2016, 23(10): 2630－2637. DOI: 10.1007/s11771-016-3324-5.

[36] ABD ELMABOUD Y , ABDELSALAM S I, MEKHEIMER K S, VAFAI K. Electromagnetic flow for two-layer immiscible fluids [J]. Engineering Science and Technology, an International Journal, 2019, 22(1): 237 － 248. DOI: 10.1016/j.jestch.2018.07.018.

[37] MISRA J C, PANDEY S K. Peristaltic flow of a multilayered power-law fluid through a cylindrical tube [J]. International Journal of Engineering Science, 2001, 39(4): 387−402. DOI: 10.1016/S0020-7225(00)00038-0.

[38] AWAN S E, AWAIS M, RAJA M A Z, PARVEEN N, ALI H M, KHAN W U, HE Yi-gang. Numerical treatment for dynamics of second law analysis and magnetic induction effects on ciliary induced peristaltic transport of hybrid nanomaterial [J]. Frontiers in Physics, 2021, 9: 631903. DOI: 10.3389/fphy.2021.631903.

[39] PACHERRES C O, AHMERKAMP S, SCHMIDT-GRIEB G M, HOLTAPPELS M, RICHTER C. Ciliary vortex flows and oxygen dynamics in the coral boundary layer [J]. Scientific Reports, 2020, 10: 7541. DOI: 10.1038/s41598-020-64420-7.

[40] BHATTI M M, ELELAMY A F, SAIT S M, ELLAHI R. Hydrodynamics interactions of metachronal waves on particulate-liquid motion through a ciliated annulus: Application of bio-engineering in blood clotting and endoscopy [J]. Symmetry, 2020, 12(4): 532. DOI: 10.3390/sym12040532.

[41] SIDDIQUI A, ZEB M, HAROON T, AZIM Q U A. Exact solution for the heat transfer of two immiscible PTT fluids flowing in concentric layers through a pipe [J]. Mathematics, 2019, 7(1): 81. DOI: 10.3390/math7010081.

(Edited by HE Yun-bin)

中文导读

外周层纤毛运动引起的PTT流体流动的热和浓度分析

摘要：本文分析了两层纤毛诱导的Phan-Thien-Tanner (PTT)流体的热效应和浓度效应。采用Phan-Thien-Tanner流体模型模拟呼吸道黏液。由于呼吸道上皮细胞上存在睫状体周液层(PCL)和气道睫状体层(ACL)，因此采用两层模型方法进行模拟。采用长波长和小雷诺数近似简化了两层流动问题的数学模型，所得到的带有移动边界的微分方程给出了两层中速度、温度和浓度分布的精确解。采用速度分布计算了压力的变化，并采用沿通道壁面压力梯度的数值积分计算了压力的上升。利用曲线图说明了物理参数对压力上升、速度、温度和浓度分布的影响。结果表明：流体内层(PCL)的速度和温度分布最大，流体外层(ACL)的浓度分布最大。

关键词：纤毛流；PTT流体；两层模型；热分析；浓度效应